Paleontological Research

Papers in Press

"Papers in Press" includes peer-reviewed, accepted manuscripts of research articles, reviews, and short notes to be published in Paleontological Research. They have not yet been copy edited and/or formatted in the publication style of *Paleontological Research*. As soon as they are printed, they will be removed from this website. Please note they can be cited using the year of online publication and the DOI, as follows:

Humblet, M. and Iryu, Y. 2014: Pleistocene coral assemblages on Irabu-jima, South Ryukyu Islands, Japan. *Paleontological Research*, doi: 10.2517/2014PR020.

doi:10.2517/2019PR007

Morphometric analysis of two Eocene related radiolarian species of the *Podocyrtis* (*Lampterium*) lineage

Taniel DANELIAN[1], Norman MacLEOD[2]

[1] Université Lille, CNRS, UMR 9198 - Évo-Éco-Paléo, F-59000 Lille, France (e-mail : taniel.danelian@univ-lille.fr)

[2] Department of Earth Sciences, The Natural History Museum, Cromwell Road, London, SW7 5BD, United Kingdom

Abstract.

A metric analysis of the morphology of two related Eocene species (*Podocyrtis sinuosa* and *P. mitra*) that are part of the *Lampterium* evolutionary lineage was undertaken in order to evaluate hypotheses related to their mutual taxonomic distinction statistically. All analyses (landmark, outline semi-landmark and landmark-constrained outlines) support an interpretation of statistically significant species-specific shape differences. Moreover, landmark and semilandmark-based morphometric characterizations can be used to identify which regions of the test are best suited for making reliable taxonomic distinctions. These results suggest that both abdomen and thorax shapes represent species-specific characters. While this agrees, in part, with previous, qualitative diagnoses, our results shed light on precisely how abdomen and thorax shape differ between these species. In addition, our investigation demonstrates the taxonomic value of a morphometric approach to character analysis as thorax shape differences had gone unnoticed by previous investigators.

Key words: Eocene, evolutionary lineage, geometric morphometrics, radiolaria, test shape

Introduction

Radiolaria are marine planktonic and heterotrophic protists that live in all modern oceans. Although found at every depth in the marine water column, radiolarians exhibit several depth-related trophic strategies (Matsuoka, 2007). Polycystine radiolaria secrete siliceous skeletons that are preserved commonly in deep-sea sediments. With a fossil record extending from the Early Cambrian (Obut and Iwata, 2000; Pouille *et al.*, 2011; Aitchison *et al.*, 2017) radiolaria can be used to explore plankton skeletal evolution in deep time (Kellogg, 1976, 1983; Prothero and Lazarus, 1980; Lazarus, 1985, 1986; Motoyama, 1997; Hatakeda *et al.*, 2007).

Podocyrtis sinuosa and *P. mitra* were first described by Ehrenberg in the 19th century (Ehrenberg 1874, 1876) based on material from Barbados. However, it is only following the work of Riedel and Sanfilippo (1970) on radiolarian assemblages collected from southern Caribbean drill cores (Venezuela Basin, DSDP Site 29) that the taxonomic concepts and evolutionary relationship between these species were clarified (see also Sanfilippo *et al.*, 1985; Sanfilippo and Riedel, 1992; Nigrini and Sanfilippo, 2001).

Both species are characterized by a horn-bearing cephalis, a campanulate thorax, an abdomen and three feet (Figure 1). The main qualitatively recognized difference between them has been the overall shape of the abdomen. According to Riedel and Sanfilippo, *Podocyrtis mitra* is distinguished from *P. sinuosa* by having the greatest width of the abdomen placed distally, toward the feet, forming a vase-shaped abdominal outline rather than medially, equidistant from the abdominal-thorax stricture and the distal terminus of the abdomen, forming a truncated circular outline. *Podocyrtis mitra* has been described as having originated from *P. sinuosa* via anagenetic transformation, both morphospecies being part of the *Podocyrtis* (*Lampterium*) lineage (Riedel and

Sanfilippo, 1970; Sanfilippo *et al.*, 1985; Sanfilippo and Riedel, 1992). Interestingly, biostratigraphic data indicate that these two abdominal morphologies show a substantial time interval of co-occurrence. At the beginning of the stratigraphic interval in which both morphospecies co-occur, *P. sinuosa* specimens are usually more abundant than those of *P. mitra*. The horizon at which *P. mitra* becomes relatively more abundant than *P. sinuosa* is biostratigraphically important as it defines the base of the Radiolarian Biozone RP14 (Sanfilippo and Nigrini, 1998). However, in this transitional interval, which may be as thick as 30 m in areas characterized by high sediment-accumulation rates (i.e., Leg 207; Danelian *et al.*, 2005, 2007), RP14 is often difficult to locate precisely because of the presence of numerous intermediate morphotypes. Accordingly, a more reliable and detailed geometric description of the diagnostic differences that separate *P. sinuosa* and *P. mitra* is needed to facilitate both accurate and consistent biostratigraphic analysis. In a later work on the quantitative discrimination of Eocene radiolaria, Sanfilippo and Riedel (1990) used shape coordinates to test whether *Podocyrtis* morphospecies could be discriminated quantitatively. Our study extends this initial investigation by combining information from both contour/outline and landmarks in a comparative analysis of *P. sinuosa* and *P. mitra* (Figure 1).

More particularly, in this investigation we focused on testing the following questions.

1. Can the test shapes of *Podocyrtis mitra* and *P. sinuosa* populations, as identified by taxonomic experts, be distinguished objectively and consistently from one another?
2. What regions of the test are important for making distinctions between these two species?

Material and Methods

The material analysed consisted of 60 specimens of *Podocyrtis sinuosa* and 54 specimens of *P. mitra* (see Table 1 and Figure 2). Part of this material came from three different stratigraphic levels in a core collected from the tropical Atlantic ODP Site 1259A (Erbacher *et al.*, 2004); sample 1259A-25R-cc which contains only specimens that can be assigned qualitatively to *P. sinuosa* and sample 21R-cc which contains only specimens of *P. mitra*. Sample 24R-cc contains specimens that can be assigned qualitatively to either morphospecies. This study material was enriched via inclusion of typical *P. mitra* from the Indian Ocean DSDP Site 709C (Johnson, 1990) and typical *P. sinuosa* from the Caribbean DSDP Site 94 (Sanfilippo and Riedel, 1973).

In order to capture the types of comparisons radiolarian taxonomists make routinely when identifying these species their 2D geometries were assessed using a combination of landmarks and outlines represented by semilandmarks (Bookstein, 1991). The landmarks (Figure 1) included the distal tip of the cephalis, stricture between cephalis and thorax, stricture between thorax and abdomen, and distal terminus of abdomen. Positions of the lateral termini of the maxima abdominal chord as measured from the axis of test symmetry were also recorded as part of the landmark dataset, as these points have been considered critical for qualitative species diagnosis. These landmarks were located individually without requiring that they be placed at the same positions along the axis of symmetry on either side of the test. The base of the horn, along with the cephalis, thoracic and abdominal structure landmarks located along the left and right limbs of the test outline, were also used to parse a 200-point trace of the test outline into six homologous outline segments, with the shapes of these outline segments being represented by a series of equally-spaced semilandmark coordinate points whose inter-point spacing was consistent within segments but differed between segments according to the complexity of the curve outline (see MacLeod, 1999). Abdominal outline segment limbs were represented by five semilandmark coordinate points, the

thoracic segments by five semilandmark coordinate points, and the cephalic segments by four semilandmark coordinate points. This representation scheme ensured that geometries of all outline curve segments were reproduced to a length-fidelity ratio of at least 95 percent across the entire sample (see MacLeod, 1999). For the outline dataset no attempt was made to constrain the geometry of the abdominal segment limbs by marking the position of the maximal abdominal segment width landmarks as the positions of these points are often difficult to determine precisely and consistently from investigator to investigator. Nevertheless, the outline sampling fidelity of the abdominal (as well as the thoracic and cephalis) segments was such that geometric regularities in the shape of these outlines were captured and used in our metric comparisons.

A geometric morphometric investigation of these data was undertaken using a common approach to the analysis of landmark data, semilandmark data and combined landmark and semilandmark datasets in order to render all results comparable. This procedure goes by various names (e.g. relative warp analysis, Procrustes PCA, coordinate-point eigenshape analysis), but always involves a preliminary alignment of the landmark/semilandmark coordinate configurations via the mathematical Procrustes procedure (Rohlf and Slice, 1990) followed by a subsequent principal components analysis (PCA) of the aligned shape coordinates. The former procedure corrects the raw coordinate data for variation due to position, rotation and scale while the latter creates a set of latent (eigen) vectors which are mutually orthogonal and aligned with the directions of maximum shape variance in the pooled dataset. Application of PCA is also commonly employed to reduce the dimensionality of the dataset via repackaging of the raw variables and minimizing computational problems associated with collinearity.

This Procrustes PCA data-analysis procedure was applied to the entire set of coordinate-point data collected from each specimen and to subsets of these data corresponding to the shapes of the cephalis, thorax, and abdomen. In each case the PCA decomposition was used to define a series of

sample-specific shape variables that together represented at least 95 percent of each dataset's shape covariance structure. For each dataset, projections (scores) of the original data onto the first *n* PC axes that, together, represented at least 95 percent of shape-variation structure were then submitted to a canonical variates analysis (CVA) in order to construct a linear vector that maximally separated group centroids relative to within-group dispersion matrices (see MacLeod, 2007a). The ability of these discriminant functions to separate the individuals identified *a priori* as belonging to either species on qualitative morphological criteria was assessed quantitatively by comparing a cross-tabulation of specimens assigned *a posteriori* to species groups based on their Mahalanobis distances from the two group centroids (see MacLeod, 2007b) and statistically using both parametric and bootstrapped versions of Hotelling's T^2 test (MacLeod, 2007a) in order to ensure that our interpretation of these results was robust to both distributional assumptions inherent in this multivariate test (see Manly, 2006) and to sample size-dimensionality issues inherent in the use of CVA to analyze morphometric data (see Mitteröcker and Bookstein, 2011; MacLeod, 2015, 2018). Interpretation of the results of the CVA was facilitated via calculation of shape-difference models using the procedure described by MacLeod (2002a, b, 2005).

Results

All Segments (Landmark and Semilandmark data)

Geometric analysis of all six outline segments indicated that 95 percent of the shape-variation structure in the pooled *Podocyrtis mitra* - *P. sinuosa* dataset could be represented by eight linear shape vectors (Supplementary data 1). A scatterplots formed from the three most important PC eigenvectors (Figure 3) indicated poor separation between the two morphospecies with an extensive region of overlap between the fields that represent regions of species-specific test shape variation. This result is somewhat counterintuitive insofar as the sample was composed only of typical

representatives of both species. Nevertheless, the large region of overlap in the outline shapes exhibited by these species is fully indicative of the level of difficulty taxonomists would be expected to encounter when trying to identify these species based on qualitative assessments of their test morphologies.

Podocyrtis mitra appears the more distinct within both the PC-1 *vs* PC-2 and PC-2 *vs* PC-3 shape planes. Also, the fact that maximal between-species shape separation was recorded predominantly along PC-1 suggests that species-specific shape differences are an important factor in controlling the directors of pooled shape variation in this sample. But these ordinations indicate that factors other than, or in addition to, taxonomy are playing substantial roles in determining the major directions of shape variation in this sample.

In order to maximize the expression of species-specific test shape distinctions in these data scores the first eight PC eigenvectors (= 95.08% of observed shape variance) were submitted to a subsequent CVA. This operation enabled all of the information included in these dimensions to be included in the discriminant analysis and the shape data transformed into a space that maximized between-species shape distinctions relative to within-species shape dispersions. Because there are only two groups involved in this analysis only one discriminant vector (or axis) is needed to summarize species-specific test shape distinctions.

As can be seen in Figure 4, when CVA was applied to the shape-variation patterns recorded by all eight eigenvectors, these data were able to be combined into a single synthetic variable that dramatically reduced the region of morphological overlap between these two species' distributions of shape variation. Whereas a majority of the *Podocyrtis sinuosa* specimens, and a significant number of the *P. mitra* species were located in a broad region of overlap within spaces formed by the first three PC eigenvector axes, only a small region of overlap actually characterizes these two species in our sample when the influence of factors not related directly to taxonomy is minimized.

This result clearly suggests that these two species should be objectively diagnosable on the basis of test overall test-morphology data. Comparisons between Figures 3 and 4 also illustrate why PCA ordination plots should never be used to assess the distinctions among groups included in a sample (see MacLeod, 2015, 2018).

Once an optimal linear species-specific discriminant vector had been located within the eight-dimensional space formed by the PC axes, individual shapes were assigned to groups post hoc, by determining the proximity of the individual shapes' projected positions in the discriminant space to the positions of each group centroid. While not strictly a statistical exercise, this procedure provides a useful guide to the overall quality of the between-groups discrimination achieved and for the purpose of identifying either atypical specimens and/or those of intermediate/indeterminate taxonomic assignment. A summary of these comparisons is typically tabulated in the form of a contingency table, also known as a "confusion matrix".

Although the sample was small, our discriminant axis appears to be highly reliable, classifying 98.1 percent of the training set sample of *Podocyrtis sinuosa* correctly post hoc and 94.44% of *P. mitra*. This raw result demonstrates that the distribution of morphologies between the two species in our sample, as assessed by our landmark-semilandmark data, is overwhelmingly disjunct. Identical values were obtained from a jackknife simulation test of this result indicating that the discriminant-function result is not a consequence of the discriminant function being overfit to these data and that this function is stable with regard to minor variations in the sample composition.

The separation between species-specific shape means relative to their variances along the CV-1 axis was tested using both a parametric and bootstrap variant of the Hotelling T^2 test (Supplementary data 2). Results of these tests indicated that the species separation shown in Figure 4 is significant at a very high level of confidence ($\alpha << 5.0$ %) irrespective of distributional assumptions made about

these data. The fact that the bootstrap test rejected the null hypothesis or that no significant between-group difference exists also suggests strongly that our discriminant result cannot be discounted on the basis of sample size-dimensionality interactions, at least for the sample under consideration.

Contribution of individual segments to overall species discrimination

The following section presents results of a separate analysis of the *Podocyrtis* abdomens, thorax and cephalis in order to assess how each of these regions contributes to overall species discrimination.

Abdomen.-

Geometric analysis of the two test outline segments representing the lateral margins of the abdomen's shape indicated that 95 percent of the shape variation in the *Podocyrtis mitra* - *P. sinuos*a dataset can be represented by four shape axes (Supplementary data 1). A scatterplot of the two most important PC eigenvector axes (Figure 5) indicates that a good distinction between the two morphospecies is captured by this combination of eigenvector axes with a comparative small region of species-specific overlap.

Scores on the first four PC eigenvectors (95.89 % of observed shape variance) were submitted to a CVA. Figure 6 illustrates the result of a discriminant analysis of the two species, based only on the shape of the abdomen. While the degree over overlap exhibited by two species along the optimal linear discriminant vector for the abdomen data is larger than for the whole-test result (compare with Figure 4), the overwhelming majority of abdomen shapes in our sample occupied mutually

exclusive regions of the species-specific shape space. The raw confusion matrix calculated for this result suggests that this discriminant axis appears to be very reliable overall, classifying 90.7 percent of the training set sample of *Podocyrtis sinuosa* correctly post hoc (91.6 % of the jackknifed analysis) and 96.3 percent of *P. mitra* (92.6 % of the jackknifed analysis). These results suggest that the distribution of abdominal shapes between typical representatives of these two species is predominantly disjunct, a finding that agrees well with previous qualitative and quantitative assessments. The highly reliable values obtained for the jackknife result (as opposed to the raw, or training set, confusion matrix values) also indicate that this discrimination is not a consequence of overfitting due to high dataset dimensionality and low sample size.

These shape-distribution results are further confirmed statistically by Hotelling's T^2 tests which rejected the null hypothesis of no difference in the mean group vectors relative to their within-group shape variance at a high level of statistical confidence ($\alpha << 0.05$; see Supplementary data 2). Comparison of the magnitude of the T^2 test statistic to that obtained for the all-segments analysis (Supplementary data 2) shows that the result obtained from the abdomen is superior to that obtained for all the segments, owing no doubt to the absence of the taxonomically more ambiguous cephalis and thorax shape data.

Comparison of Figure 6 with the shape models calculated at positions along CV-1 shows that *Podocyrtis mitra* differs from *P. sinuosa* primarily in terms of the distinctly conical character of its abdominal shape, with the maximum of peripheral curvature being displaced strongly toward the distal end of the segment. This result also supports the conclusions regarding abdomenal shape distinctions reached or alluded to by previous investigators.

Thorax.-

Geometric analysis of the two test-outline segments assigned to represent thorax shape suggests that 95 percent of the shape variation in the *Podocyrtis mitra – P. sinuosa* dataset can be represented in five shape axes (Supplementary data 1). A scatterplot of the two most important of these linear shape-variation eigenvector axes (Figure 7) suggests that this aspect test morphology exhibits a moderately good distinction between these two species. The character of this difference is quite interesting insofar as no qualitative taxonomist has suggested previously that the shape of the thorax, in addition to that of the abdomen, might be used to achieve a reliable diagnosis for any *Podocyrtis* species.

As with the previous analyses, the character of overall discrimination is improved by inclusion of the additional three eigenshape axes required to represent 95.52 percent of the observed shape variation in a formal discriminant analysis. A histogram summarizing the pattern of group-specific shape variation along the single linear discriminant axis shows a surprisingly good discrimination (Figure 8). Indeed, it would appear that, in our sample of typical *Podocyrtis sinuosa* and *P. mitra* specimens, thorax shape has the ability to distinguish between the identities of these two species almost as well as an analysis employing all test segments. Based on the confusion matrix for these thorax outline data, the discriminant axis appears to be fairly reliable, classifying 85.19 percent of the training set sample of *P. sinuosa* correctly post hoc (88.89 % in the jackknifed analysis) and 90.74 percent of *P. mitra* (85.18 % in the jackknifed analysis). These results suggest that the distribution of thoracic morphologies in these two species, contains surprisingly few intermediates. The significant of this result is further confirmed by both parametric and bootstrapped Hotelling's T^2 tests which rejected the null hypothesis of no difference between mean values between the two samples to a high level of statistical confidence ($\alpha << 0.5$; see Supplementary data 2).

The sequence of shape models calculated for the CV-1 axis (Figure 7) shows that the characteristic *Podocyrtis mitra* thorax differs from that of *P. sinuosa* primarily in its greater relative height and

subequality of transverse lengths of the proximal and distal strictures. In addition, the relative degree of inflation as assessed by the curvature of the thorax outline segments is typically higher in *P. sinuosa* compared to *P. mitra*. Thus, isolation of the thorax enables an important distinction between segment inflation as a result of differences between proximal/distal stricture lengths, and inflation as a result of segment periphery curvature, to be recognized. It is also worth noting that this difference is not evident in the total outline results, presumably because of the influence of the abdomen and cephalis shape variation in the latter analysis.

Cephalis.-

Geometric analysis of the test outline segments assigned to represent cephalis shape indicates that 95 percent of shape variation in the *Podocyrtis mitra – P. sinuosa* dataset can be represented in five linear shape eigenvectors (Supplementary data 1). Nevertheless, a scatterplot of the two most important of these linear shape variation axes (Figure 9) displays an almost complete overlap between the shape distributions of these two species within the PC-1 vs PC-2 shape plane. This result suggests there exists little distinction between these two species on the basis of cephalis shape alone. A histogram summarizing the pattern of groups-specific shape variation along the single discriminant axis shows also no obvious species-specific cephalic shape discrimination (Figure 10).

Consistent with the large area of overlap for this character shown in figures 8 and 9, based on the calculated confusion matrix for this discriminant result, cephalis shape discriminant axis appears to be a relatively poor indicator of taxonomic difference, classifying only 64.81 and 66.67 percent of the training set sample of training set *Podocyrtis sinuosa* and *P. mitra* specimens (respectively) correctly post hoc with 64.81 and 61.11 percent correct identification on the basis of the more rigorous jackknife resampling strategy. These results suggest that, while the distribution of

morphologies between the two species is somewhat disjunct, at least in our sample, species-specific differences in this region of the test would likely prove an unreliable basis for making any critical identifications unless abdominal and/or thoracic data were unavailable. Interestingly, both parametric and bootstrapped Hotelling's T^2 tests of these cephalis CV-1 score data rejected the null hypothesis of no difference between the mean difference in the CV-1 score values at an appropriately a high level of statistical confidence ($\alpha << 0.5$; see Supplementary data 2). Thus, the cephalic shape differences illustrated in Figure 10 are regarded as being significant statistically. But the statistical significance of mean vector differences, and the performance of discriminant functions, are separate issues in the overall interpretation of group differences. On overall consideration, these results strongly suggest that identifications between these two species based on cephalic-shape data along are likely to be unreliable taxonomically.

Landmark data

A landmark analysis was also conducted in order to provide a basis of comparison with the outcome of the "all segment" shape analysis, discussed above. The key difference between these two datasets is that, for the landmark dataset, an additional landmark was placed at the maximal extent of each abdomen limb laterally, whereas for the outline dataset landmarks were only placed at the cephalis/thorax and thorax/abdomen strictures, along with the endpoints of the abdomen. Between these landmarks curves were represented with semilandmarks, five on either side of the abdomen, five on either side of the thorax and four on either side of the cephalis. Therefore, the landmark dataset tests the consistency with which the points represents the maximal lateral extent of the abdomen can be located and their role of these points in facilitating discrimination between these two species relative to the more traditional qualitative assessments of cephalic and thoracic shapes.

Geometric analysis of these landmark data indicated that 95 percent of shape variation in the *Podocyrtis mitra* - *P. sinuos*a dataset can be represented by seven eigenvector axes (Supplementary data 1). Interestingly, a scatterplot of the two most important eigenshape axes for these data (Figure 11) indicates that an excellent distinction between the two morphotypes was captured predominantly along the first (PC-1). The first seven eigenvectors (95.63 % of observed shape variance) were then submitted to canonical variates analysis. Figure 12 illustrates the result of the discriminant analysis of these two species based only on their test landmarks. Based on the confusion matrix, the discriminant axis appears to be very reliable, classifying 100.00 percent of the training set sample of *P. sinuosa* correctly post hoc (100.0 % is equally the result of the jackknifed analysis) and 100.00 % of *P. mitra* (100.00 % of the jackknifed analysis). The raw result suggests that the distribution of morphologies between the two species as represented by these landmark data and with reference to our sample of typical specimens, is completely disjunct. This result was confirmed statistically using the Hotelling's T^2 test which rejected the null hypothesis of no

difference in the mean group vectors relative to their within-group shape variance at a high level of statistical confidence ($\alpha << 0.05$; see Supplementary data 2).

Inspection of the CV-1 shape models that represent the landmark-defined morphological differences between *Podocyrtis sinuosa* and *P. mitra* confirms the results of the landmark and outline-based analysis described above. Inspection of migration patterns among the five landmarks that represent each limb of the test periphery indicated the position of the cephalic apex landmark was completely unchanged across all positions along CV-1. The cephalis-thorax landmark exhibited a modest proximal and inboard translation in the passage from a typical *P. sinuosa* morphology to the typical *P. mitra* morphology rendering the *P. mitra* ceaphalis both shorter in relative length and narrower in relative width relative to the *P. sinuosa* morphology. The thorax-abdomen landmark exhibited a much stronger proximal and inboard translation in the passage from a typical *P. sinuosa* morphology to the typical *P. mitra* morphology rendering the *P. mitra* thorax much shorter in relative length and much narrower in relative width to the *P. sinuosa* morphology. As was the case with the landmark-outline dataset, the differences between the thoracic shapes of these two species is very marked and very clear. The abdomen maximum lateral extent landmark also exhibited a marginally stronger distal and inboard translation in the passage from a typical *P. sinuosa* morphology to the typical *P. mitra* morphology, rendering the *P. mitra* thorax much longer in relative length and much narrower in relative width with respect to the *P. sinuosa* morphology.

As has been noted by previous investigators, and in the previous landmark-outline results, this is clearly the most marked shape distinction evident in the comparison between these two species. However, whereas Sanfilippo and Riedel (1992) characterized this transition has involving the distal migration of the maximum lateral extent landmark, our results show that this migration is also characterized by an equally important inboard translation, thus forcing the *Podocyrtis mitra* test to exhibit a much narrower shape relative to its lineal predecessor. This aspect of the distinction

between *P. sinuosa* and *P. mitra* can be difficult to appreciate owing to confounding effect of size differences between them. However, once size is removed from consideration — as it can be in a geometric morphometric analysis — the resulting improvement in the appreciation of the true nature of shape differences that exist between these two species is really quite striking and obvious.

Finally, the distal abdomen landmark exhibits predominantely inboard translation in the passage from a typical *Podocyrtis sinuosa* morphology to the typical *P. mitra* morphology with very little migration in an axial direction. This renders the overall *P. mitra* abdomen shape as exhibiting a much longer relative length, and much narrower in relative width with an strong, asymmetrical vergence of the abdomen's maximal lateral extent distally to position from 60–80 percent of the way down the abdominal axis. This geometry is most reminiscent of an inverted hyperbolid conic section with strong asymmetrical development of the length as represented by the axial position of maximum lateral extent and a much lesser, though noticeable, asymmetrical development of the abdomen's proximal and distal width in which the former exhibits the lesser value. Again, these morphologically complex shape translations are difficult to appreciate in their entirety without a guidance afforded by careful morphometric analysis owing (primarily) to the confounding effect of species-specific size differences.

Discussion

The two species analysed here are part of the *Lampterium* subgenus, a lineage with a rich fossil record that displays continuous morphological change through time, originating from a *Podocyrtis papalis* stock, first with *P. aphorma* and evolving anagenetically via *P. sinuosa* to *P. mitra* and finally to *P. chalara* (Riedel and Sanfilippo, 1970). Previously, the distinction between *P. sinuosa* and *P. mitra* had been based on the abdomen's shape: a barrel shaped abdomen for *P. sinuosa* and an elongated, inverted and asymmetrically developed conical hyperboloid (previously described,

somewhat ambiguously, as a "vase shape") for *P. mitra*,. However, as stressed by Sanfilippo and Riedel (1990, p. 347),

"conventional descriptions and diagrams are unable to accommodate all the variation and all the intermediate forms included in each species at each level in the continuum. They illustrate only the general form at a single level during the range of that particular species. The data necessary to describe the variation cannot be illustrated this way. Techniques developed for morphometric studies provide a uniform way of describing the variation and transformations involved in the evolution of these forms".

These authors applied a shape coordinate analysis to describe variation in a number of traditional *Podocyrtis* morphospecies in assemblages obtained from five stratigraphic levels of a middle Eocene sedimentary sequence from the Caribbean DSDP Site 29. Their results suggested that "the thoracic and lumbar coordinates contribute most to the variation" (p. 345) of the different *Podocytis* morphospecies introduced based on traditional descriptive taxonomy. However, they also found that the discrimination obtained was not satisfactory, a result that highlighted the need to assess additional information (e.g. outlines, pore sizes/shapes) to facilitate a successful differentiation of these radiolarian morphotypes.

In this investigation we have extended the methodology used by Sanfilippo and Riedel (1990), by (1) focusing on only two morphospecies -*Podocyrtis sinuosa* and *P. mitra*, (2) combining information from both contour/outline and landmark data, and (3) attempting to evaluate the utility of a new system of morphometric measurements in our effort to document difference(s) between these species. Our results establish that pronounced differences exist between many more aspects of these species' test geometries than had been suspected previously; differences of sufficient magnitude to allow them to be recognized objectively and consistently based on the shape of the landmark-delineated outline trace alone. Comparison of the scatterplot with the shape models calculated for whole test PC-1 (Figure 3) shows that, overall, *P. sinuosa* differs from *P. mitra* primarily in terms of its greater degree of inflation of the thoracic and abdominal test segments.

This inflation appears to be reflected most strongly in the distal region of the thorax and in the median region of the abdomen. In addition, it should be noted that our analysis was based entirely on the geometry of the test outline. No information about the character of the pore frames, size of the lattice pores, shape of the lattice pores, etc, was included.

When all the three segments of the test outline are included in the same analysis the assessment of shape variation must be interpreted in a holistic manner. However, in order to test hypotheses pertaining to similarities and differences in the patterns of shape variation in localized regions, those regions must be analyzed in isolation from other regions of the test. Unlike strictly landmark and other outline-based methods the combination of these data types in the manner described originally by MacLeod (1999) supports both flexibility in the choice of which parts of a specimen to include in an analysis, coupled with a precise and biologically meaningful representation of the character of morphological variation existing in these parts.

Starting with the abdomen, the results of our geometric analysis show a very good distinction between these two morphospecies, as abdomen shape alone appears to have an ability to distinguish between these two species in a manner identical to results obtained through an analysis using all test segments. This is not surprising, as it is a well-known fact that, in very many species, species-specific characteristics tend to be associated with late developmental stages. Like all nassellarians, the *Podocyrtis* skeleton would have been initiated at the cephalis with the throax and abdominal segments added distally through ontogeny.

Regarding the thorax, results obtained from geometric analysis of this test segment suggest that its shape variation is only slightly less distinctive and/or well organized than that of the abdomen. Indeed, the confusion matrix obtained for species discrimination using thorax outline shape alone

suggests that over 85 percent of the training set specimens could be classified correctly. This result is even more impressive when it is recalled that no information about the character of the pore frames, size of the lattice pores, shape of the lattice pores, etc, was included. While this remarkable result would undoubtedly diminish if the discriminant function (based on such a small sample) were to be used to classify unknown specimens, it nevertheless indicates that this feature of the *Podocyrtis* test has clear significance in terms of making taxonomic distinctions between these two species; a use that, until now, had eluded qualitative morphological analysts. Our case study illustrates how it is possible to isolate major structural components of complex biological morphologies through quantitative morphological analysis and evaluate patterns of form and shape variation in these structures in isolation from the confounding effects of variation in other regions of the overall morophology. In this way morphometric analyses were employed to develop a more detailed and comprehensive analysis of the overall morphology and increase the potential to discover new patterns of morphological variation that are valuable in taxonomy, and other, contexts (e.g., ecological, phylogenetic, developmental).

The results of geometric analysis for the cephalis showed little distinction between the two studied species. Of course, the cephalis is the smallest structure assessed in this analysis and was the structure represented by the fewest number of semi-landmark points. The cephalis is also developmentally the first to be formed and so constitutes a relatively juvenilized morphology. Cephalis shape was also likely subject to a greater degree of error insofar as the horn —which was variably preserved in this sample — was not included in the analysis, necessitating estimation of the shape of the proximal cephalic margin. While a more detailed analysis of cephalis shape could be undertaken using scanning electron microscopy, this technique is notoriously difficult to use for detailed morphometric analysis owing to difficulties in preserving precise metric relations between regions of the image frame. It is also the case that the cephalis will, in the majority of cases, be the smallest region presented to the qualitative taxonomist, who would struggle with precisely the same

analytic limitations. Because of these limitations we feel cephalis shape has little value in terms of the qualitative or quantitative discrimination of *Podocyrtis* taxa, at least for this dataset.

Conclusions

The results of this study suggest that:

1. The test shapes of *Podocyrtis mitra* and *P. sinuosa* can be distinguished objectively and consistently from one another. All the results of geometric morphometric analyses (landmark, landmark-constrained outlines) support an interpretation of statistically significant species-specific shape differences. Provided the species identifications used here are accepted, our results indicate that it is possible to construct a quantitative shape space, based on a metric assessment of linear patterns of shape variation, such that a probabilistic estimate could, in theory, be made of specimen identity based on test shape data alone.

2. Overall test shape, abdomen shape and/or thorax shape can all be used as a basis for the identification of these two species. While abdomen shape appears to be slightly more reliable than overall test shape, the results obtained for all three datasets are very similar. It will require additional analyses with larger samples in order to better capture important patterns – such as the thoracic shape difference – and to better determine differences in discrimination power that characterize these regions of the *Podocyrtis* test.

In this initial study we have not attempted to construct a method for morphometrically determining the stratigraphic ranges of either species. Rather, our goal was to make a preliminary evaluation of whether morphometric measurements can be used to identify these species and what type of measurements might be best-suited for this purpose. Our ultimate goal is to improve Eocene

radiolarian biochronostratigraphy through development of a reliable, consistent and objective method for determining these two species' range end-points both for its own sake and as a demonstration of how quantitative morphological analysis can contribute to radiolarian biostratigraphy in a practical manner.

Acknowledgments

Financial support through SYNTHESYS funding is gratefully acknowledged. It was made available by the European Community – Research Infrastructure Action under the FP6 ―Structuring the European Research Areal Programme. We are grateful to Dave Lazarus (Berlin) for his help that allowed us to study radiolarian slides stored in the DSDP-ODP collections of the Natural History Museum in Berlin. Constructive remarks by Dave Lazarus and Takao Ubukata improved the initial manuscript.

References

Aitchison, J. C., Suzuki, N., Caridroit, M., Danelian, T. and Noble, P., 2017: Paleozoic radiolarian biostratigraphy. *In*, Danelian, T., Caridroit, M., Noble, P. and Aitchison, J.C. *eds.*, *Catalogue of Paleozoic Radiolarian Genera. Geodiversitas*, vol. 39, p. 503–531. Scientific Publications of the Muséum National d'Histoire Naturelle, Paris.

Bookstein, F. L., 1991: *Morphometric Tools for Landmark Data: Geometry and Biology*, 435p. Cambridge University Press, Cambridge.

Danelian, T., Le Callonec, L., Erbacher, J., Mosher, D., Malone, M., Berti, D., Bice, K.L., Bostock, H., Brumsack, H.-J., Forster, A., Glatz, C., Heidersdorf, F., Henderiks, J., Janecek, T. J., Junium, C., MacLeod, K., Meyers, P. A., Mutterlose, J. H., Nishi, H., Norris, R., Ogg, J. G., O'Reagan, M. A., Rea, B., Sexton, P., Sturt, H., Suganuma, Y., Thurow, J. W., Wilson, P. A. and Wise, S.W.,

2005: Résultats préliminaires sur la sédimentation pélagique de l'Atlantique tropical au Crétacé et Tertiaire (plateau de Demerara, Leg ODP 207). *Comptes Rendus Géoscience*, vol. 337, p. 609–616.

Danelian, T., Saint Martin, S. and Blanc-Valleron, M.-M., 2007: Middle Eocene radiolarian and diatom accumulation in the equatorial Atlantic (Demerara Rise, ODP Leg 207): Possible links with climatic and palaeoceanographic changes. *Comptes Rendus Palevol*, vol. 6, p. 103–114.

Ehrenberg, C. G., 1874: Grössere Felsproben des Polycystinen-Mergels von Barbados mit weiteren Erläuterungen. *Monatsberichte der Königlichen Preussische Akademie des Wissenschaften zu Berlin*, Band 1873, p. 213–262.

Ehrenberg, C. G., 1876: Fortsetzung der mikrogeologischen Studien als Gesammt-Uebersicht der mikroskopischen Paläontologie gleichartig analysirter Gebirgsarten der Erde, mit specieller ücksicht auf den Polycystinen-Mergel von Barbados. *Abhandlungen der Königlichen Preussische Akademie des Wissenschaften zu Berlin*, Band 1875, p. 1–225.

Erbacher, J., Mosher, D. and Malone, D. *et al.*, 2004: Leg 207 Summary. *Proceedings of the Ocean Drilling Program, Initial Reports*, vol. 207, p. 1–89.

Hatakeda K., Suzuki N. and Matsuoka A., 2007: Quantitative morphological analysis and evolutionary history of the Middle Jurassic polycystine radiolarian genus *Striatojaponocapsa* Kozur. *Marine Micropaleontology*, vol. 63, p. 39–56.

Johnson, D.A., 1990: Radiolarian biostratigraphy in the central Indian Ocean, Leg 115. *In*, Duncan, R. A., Backman, J., Peterson, L. C. *et al.*, *Proceedings of the Ocean Drilling Program, Scientific Results*, vol. 115, p. 395–409. Ocean Drilling Program, College Station, Texas.

Kellogg, D., 1976: Character displacement in the radiolarian genus *Eucyrtidium*. *Evolution*, vol. 29, p. 736–749.

Kellogg, D., 1983: Phenology of morphologic change in radiolarian lineages from deep-sea cores: Implications for macroevolution. *Paleobiology*, vol. 9, p. 355–362.

Lazarus, D., 1985: Evolution of the Radiolarian species-complex *Pterocanium* : a preliminary survey. *Journal of Paleontology*, vol. 59, p. 183–220.

Lazarus, D., 1986. Tempo and mode of morphologic evolution near the origin of the radiolarian lineage *Pterocanium prismatium*. *Paleobiology*, vol. 12, p. 175–189.

MacLeod, N., 1999: Generalizing and extending the eigenshape method of shape visualization and analysis. *Paleobiology*, vol. 25, p. 107–138.

MacLeod, N., 2002a: Geometric morphometrics and geological form-classification systems. *Earth-Science Reviews*, vol. 59, p. 27–47.

MacLeod, N., 2002b: Phylogenetic signals in morphometric data. *In*, MacLeod, N. and Forey, P.L. *eds.*, *Morphology, shape and phylogeny*, p. 100–138, Taylor & Francis, London.

MacLeod, N., 2005: Shape models as a basis for morphological analysis in paleobiological systematics: dicotyledenous leaf physiography. *Bulletins of American Paleontology*, vol. 369, p. 219–238.

MacLeod, N., 2007a: Groups I. *The Palaeontological Association Newsletter*, vol. 64, p. 35–45.

MacLeod, N., 2007b: Groups II. *The Palaeontological Association Newsletter*, vol. 65, p. 36–49.

MacLeod, N., 2015: The direct analysis of digital images (eigenimage) with a comment on the use of discriminant analysis in morphometrics. *In*, Lestrel, P.E. *ed.*, *Proceedings of the Third International Symposium on Biological Shape Analysis*, p. 156–182. World Scientific, Singapore.

MacLeod, N., 2018: The quantitative assessment of archaeological artifact groups: Beyond geometric morphometrics, *Quaternary Science Reviews*, vol. 201, p. 319–348.

Manly, B. F. J., 2006: *Randomization, Bootstrap and Monte Carlo Methods in Biology*, *3rd edition*, 480 p., Chapman Hall/CRC, Boca Ration, Louisiana.

Matsuoka, A., 2007: Living radiolarian feeding mechanisms: new light on past marine ecosystems. *Swiss Journal of Geosciences*, vol. 100, p. 273–279.

Mitteröcker, P. and Bookstein, F. L., 2011: Linear discrimination, ordination, and the visualization of selection gradients in modern morphometrics. *Evolutionary Biology*, vol. 38, p. 100–114.

Motoyama, I., 1997: Origin and evolution of *Cycladophora davisiana* Ehrenberg (Radiolaria) in DSDP Site 192, Northwest Pacific. *Marine Micropaleontology*, vol. 30, p. 45–63.

Nigrini, C. and Sanfilippo, A., 2001: Cenozoic radiolarian stratigraphy for low and middle latitudes with descriptions of biomarkers and stratigraphically useful species, *Ocean Drilling Program Technical Note,* 27 [Online]. [cited 30 April 2018]. Available from: http://www.odp.tamu.edu/publications/tnotes/tn27/index.html.

Obut, O. T. and Iwata, K., 2000: Lower Cambrian Radiolaria from the Gorny Altai (southern West Siberia). *News of Paleontology and Stratigraphy*, vol. 2–3, p. 33–37. Suppl. to the J. Russian Geology and Geophysics, 41.

Pouille, L., Obut, O., Danelian, T. and Sennikov, N., 2011: Lower Cambrian (Botomian) polycystine Radiolaria from the Altai Mountains (southern Siberia, Russia). *Comptes Rendus Palevol*, vol. 10, p. 627–633.

Prothero, D. R. and Lazarus, D. B., 1980: Planktonic microfossils and the recognition of ancestors. *Systematic Zoology*, vol. 29, p. 119–129.

Riedel, W. R. and Sanfilippo, A., 1970: Radiolaria, Leg 4, Deep Sea Drilling Project. *In*, Bader, R.G., Gerard, R.D., *et al.*, *Initial Reports of the Deep Sea Drilling Project*, vol. 4, p. 503–575. U.S. Government Printing Office, Washington D.C.

Rohlf, F. J. and Slice, D., 1990: Extensions of the Procrustes method for optimal superposition of landmarks, *Systematic Zoology*, vol. 39, p. 40–59.

Sanfilippo, A. and Nigrini, A., 1998: Code numbers for Cenozoic low latitude radiolarian biostratigraphic zones and GPTS conversion tables. *Marine Micropaleontology*, vol. 33, p. 109–156.

Sanfilippo, A. and Riedel, W.R., 1973: Cenozoic Radiolaria (exclusive of theoperids, astrobiids and amphipyndacids) from the Gulf of Mexico, DSDP Leg 10. *In*, Worzel, J. L., Bryant, W. *et al.*, *Initial Reports of the Deep Sea Drilling Project*, vol. 10, p. 475–611. U.S. Government Printing Office, Washington D.C.

Sanfilippo, A. and Riedel, W. R., 1990: Morphometric analysis of evolving Eocene *Podocyrtis* (Radiolaria) morphotypes using shape coordinates. *In*, Rolf, F.J., Bookstein, F.L. *eds.*, *Proceedings of the Michigan Morphometrics Workshop*, p. 345–362. University of Michigan, Special Publication 2, Ann Arbor, Michigan.

Sanfilippo, A. and Riedel, W. R., 1992: The origin and evolution of Pterocorythidae (Radiolaria): A Cenozoic phylogenetic study. *Micropaleontology*, vol. 38, p. 1–36.

Sanfilippo, A., Westberg-Smith, M. J. and Riedel, W. R., 1985: Cenozoic Radiolaria. *In*, Bolli, H.M., Perch-Nielsen, K. and Saunders, J.B. *eds.*, *Plankton Stratigraphy*, p. 631–712. Cambridge University Press, Cambridge.

Figure Captions

Figure 1. Examples of the two analysed morphospecies, as well as of the 9 selected landmark points. A typical *Podocyrtis sinuosa* from the Caribbean sample 21-2-104 cm (DSDP Site 94) is illustrated on the left and a typical *P. mitra* specimen coming from the Indian Ocean sample 35X-01-28 cm (DSDP Site 709C) is illustrated on the right.

Figure 2. A selection of 14 measured specimens of *Podocyrtis sinuosa* observed in samples 94-21-2, 1259A 25R-cc and 24R-cc and of 17 measured specimens of *P. mitra* observed in samples 1259A 24R-cc, 21R-cc and 709C-35X-01.

Figure 3. Scatterplot of the two most important eigenvector axes for the entire test shape (analysis of all segments), including a representation of five models calculated for the first (= most important) shape-variation axis (PC-1).

Figure 4. Results of a canonical variates analysis for the entire test shape (analysis of all segments).

Figure 5. Scatterplot of the two most important eigenvector axes for the shape of the abdomen, including a representation of five models calculated for the first(= most important) shape-variation axis (PC-1).

Figure 6. Results of a canonical variates analysis for the shape of the abdomen.

Figure 7. Scatterplot of the two most important eigenvector axes for the shape of the thorax, including a representation of five models calculated for the first (= most important) shape-variation axis (PC-1).

Figure 8. Results of a canonical variates analysis for the shape of the thorax.

Figure 9. Scatterplot of the two most important eigenvector axes for the shape of the cephalis, including a representation of five models calculated for the first (= most important) shape-variation axis (PC-1).

Figure 10. Results of a canonical variates analysis for the shape of the cephalis.

Figure 11. Scatterplot of the first two eigenvector axes for the entire test based on nine landmarks, including the two mid-abdominal landmarks, and a representation of five models calculated for the first (= most important) shape-variation axis (PC-1).

Figure 12. Results of a canonical variates analysis for the entire test based on nine landmarks.

Table 1. Stratigraphic horizons, samples and number of specimens analysed in this study.

Supplementary data 1. Eigenvalues for the PCA analysis of Procrustes aligned shape-coordinate data.

Supplementary data 2. Results of the Hotelling's T^2 test.

Figure 1

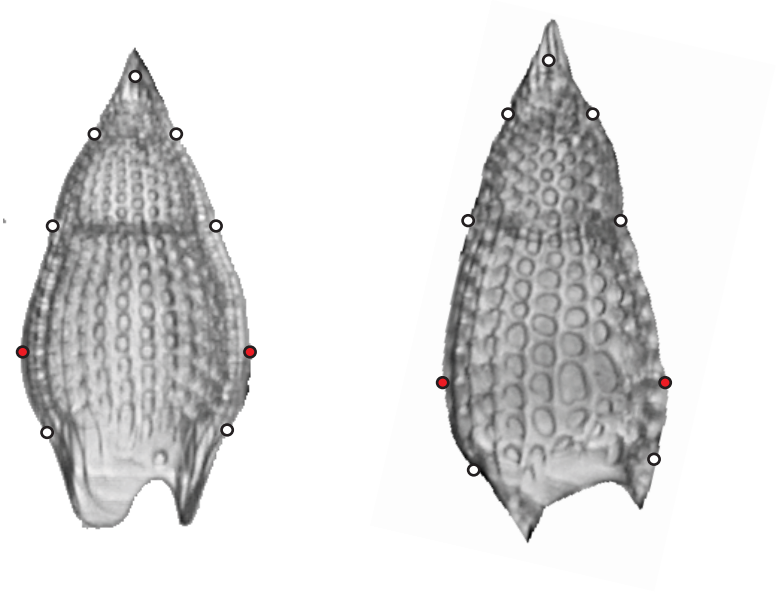

P. sinuosa

P. mitra

Figure 2

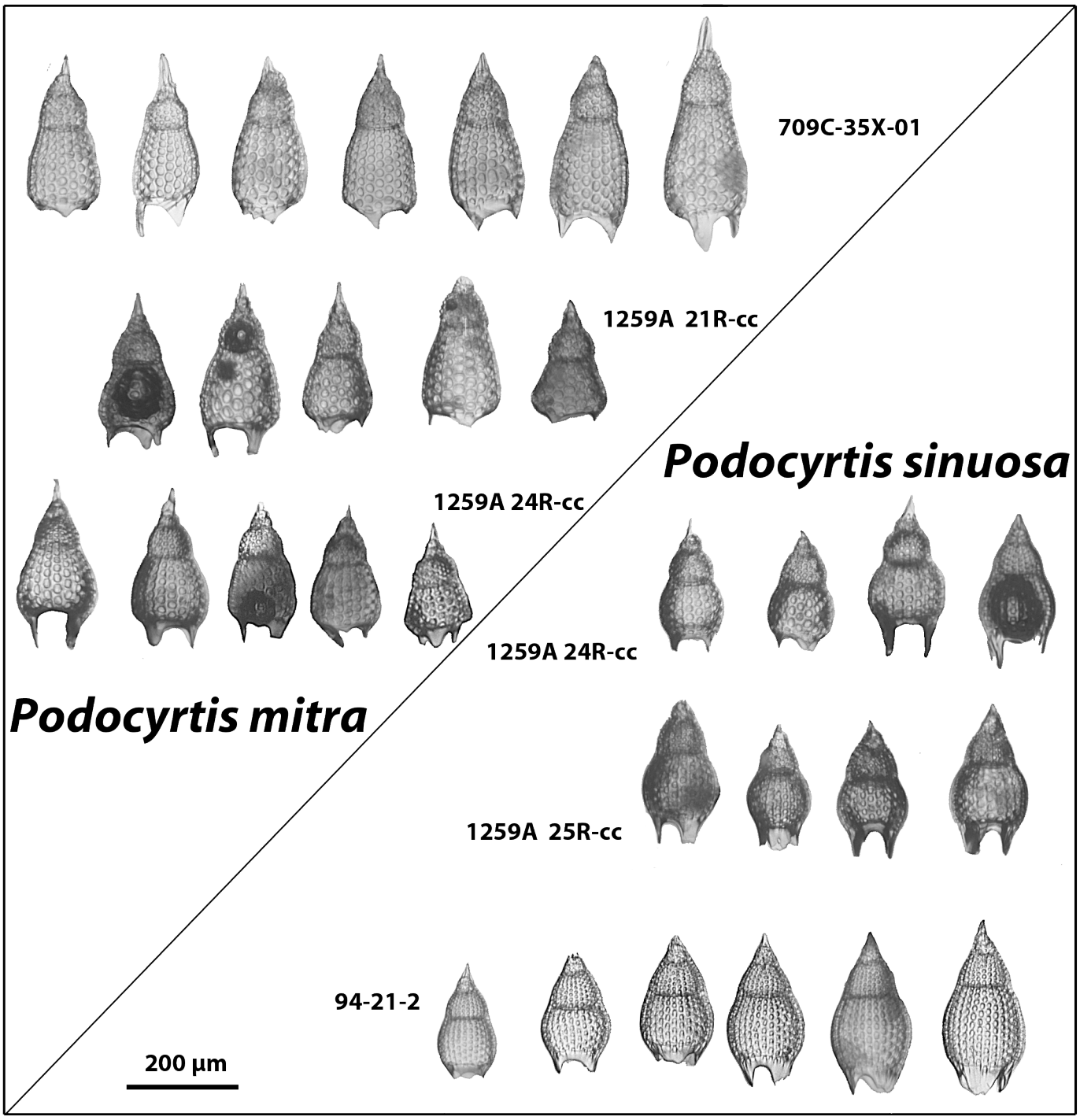
709C-35X-01
1259A 21R-cc
Podocyrtis sinuosa
1259A 24R-cc
1259A 24R-cc
Podocyrtis mitra
1259A 25R-cc
94-21-2
200 µm

Figure 3

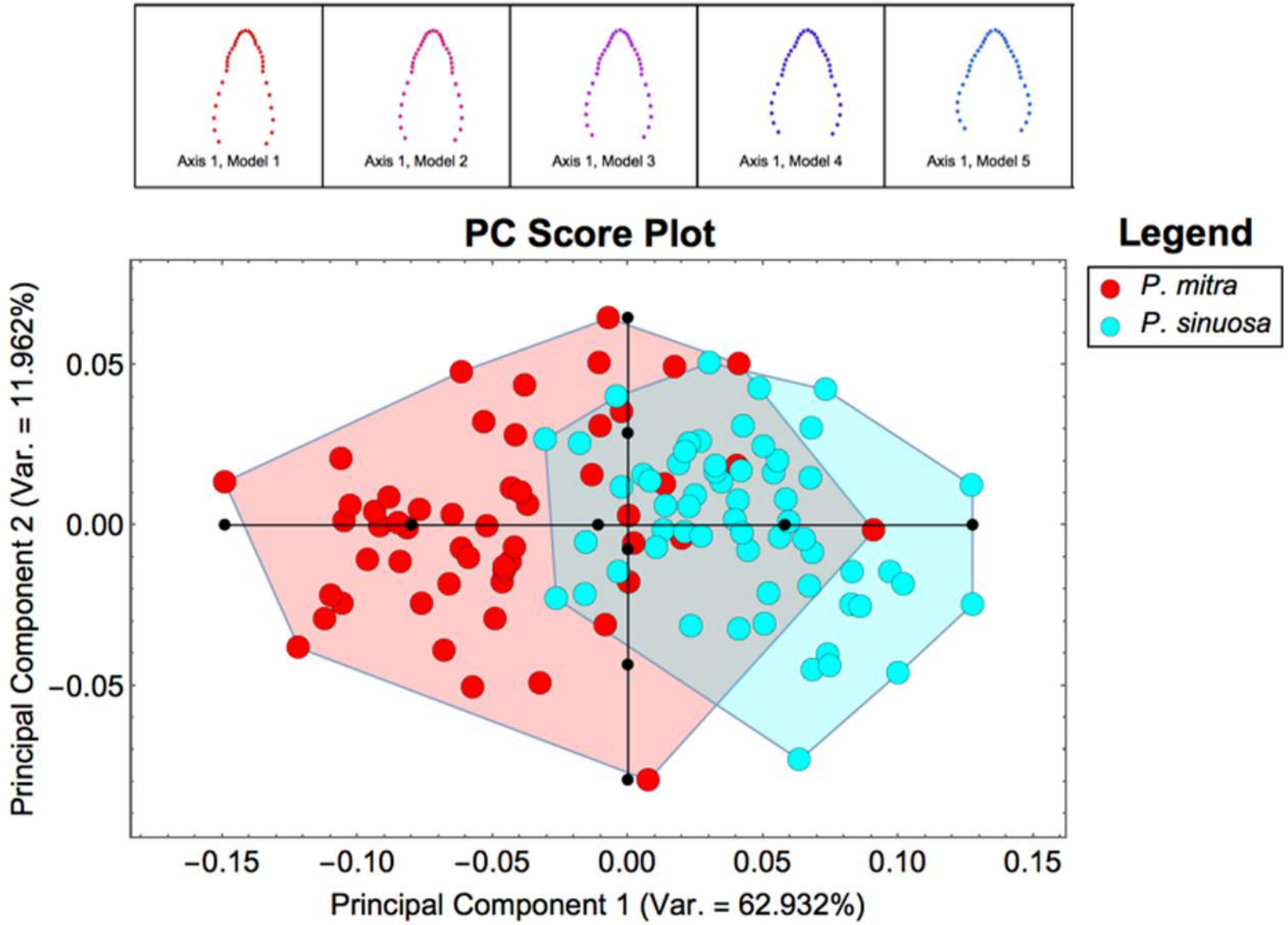
Axis 1, Model 1
Axis 1, Model 2
Axis 1, Model 3
Axis 1, Model 4
Axis 1, Model 5
PC Score Plot
Legend
P. mitra
P. sinuosa
Principal Component 2 (Var. = 11.962%)
0.05
0.00
−0.05
−0.15
−0.10
−0.05
0.00
0.05
0.10
0.15
Principal Component 1 (Var. = 62.932%)

Figure 4

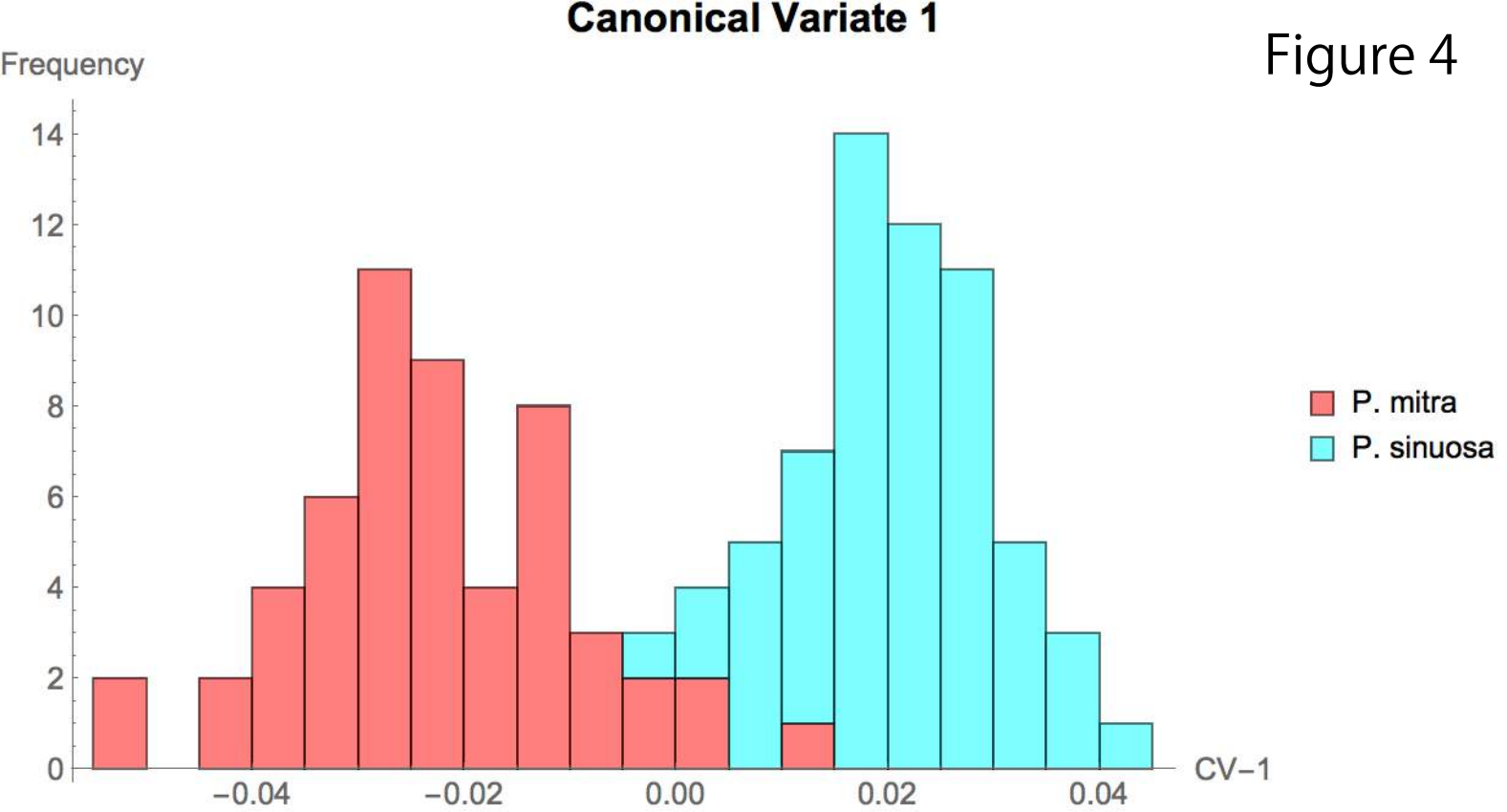
Canonical Variate 1
Frequency
14
12
10
8
6
4
2
0
−0.04
−0.02
0.00
0.02
0.04
CV−1
P. mitra
P. sinuosa

Figure 5

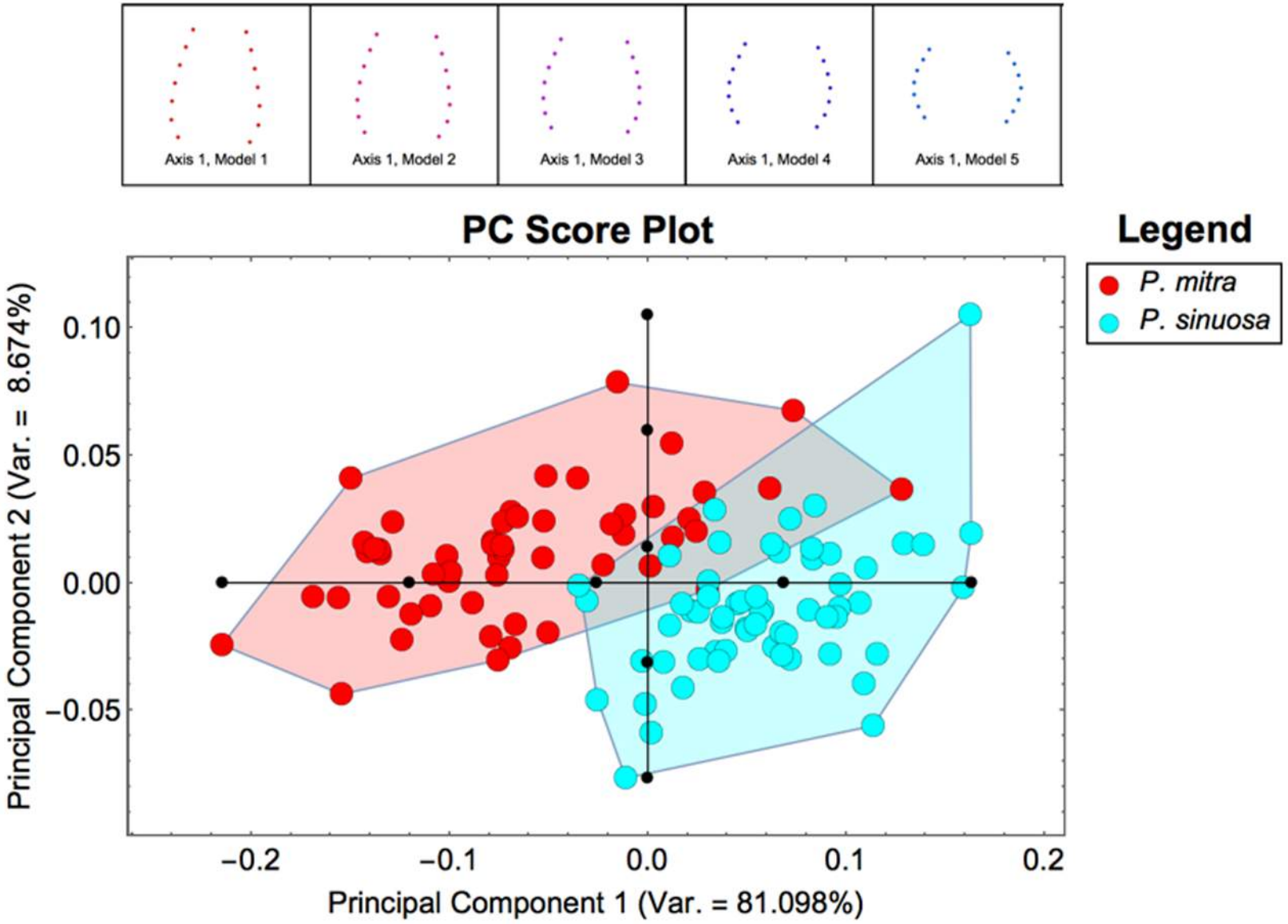
Axis 1, Model 1
Axis 1, Model 2
Axis 1, Model 3
Axis 1, Model 4
Axis 1, Model 5
PC Score Plot
Legend
P. mitra
P. sinuosa
Principal Component 2 (Var. = 8.674%)
0.10
0.05
0.00
−0.05
−0.2
−0.1
0.0
0.1
0.2
Principal Component 1 (Var. = 81.098%)

Figure 6

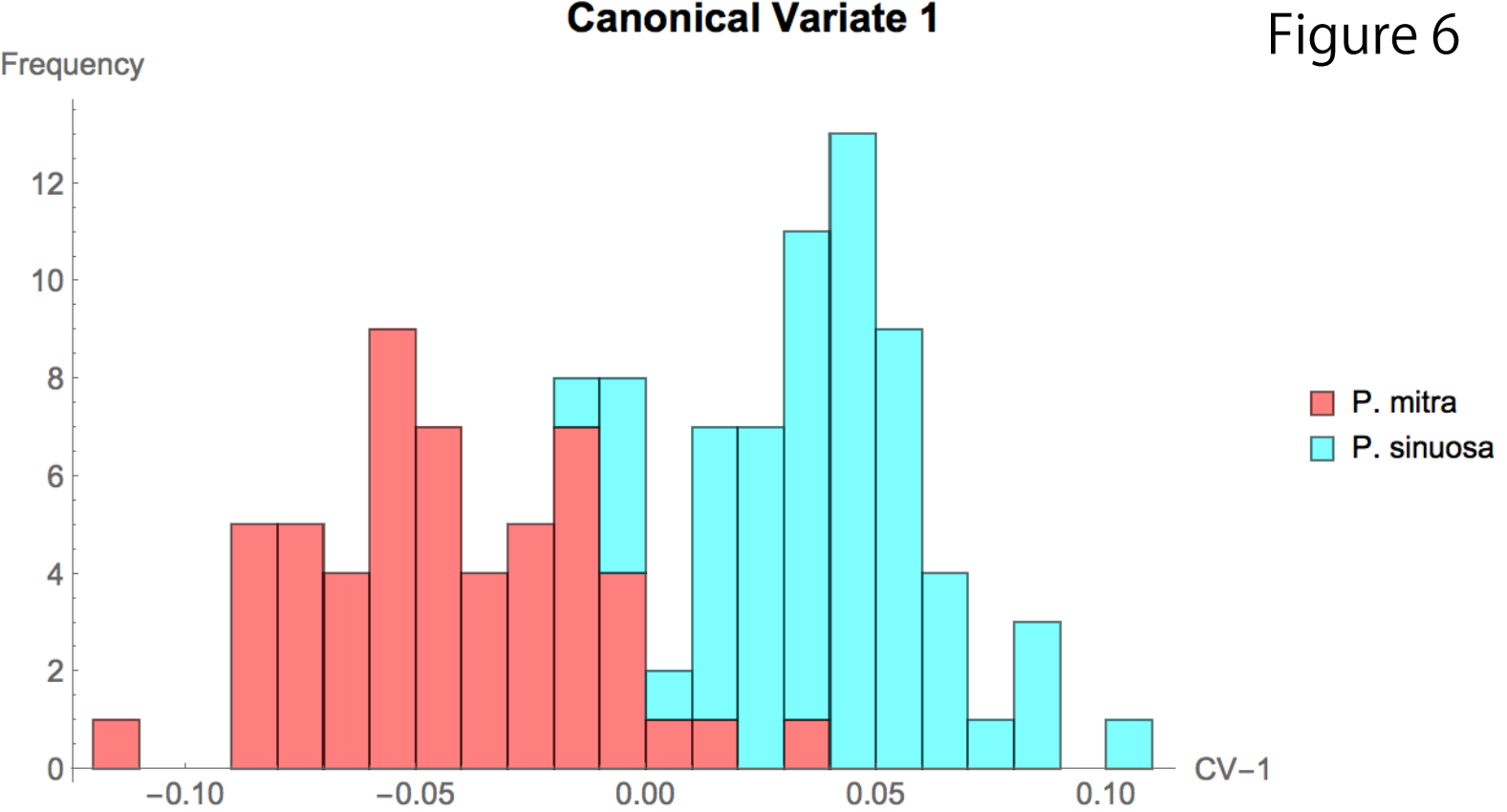
Canonical Variate 1
Frequency
12
10
8
6
4
2
0
−0.10
−0.05
0.00
0.05
0.10
CV−1
P. mitra
P. sinuosa

Figure 7

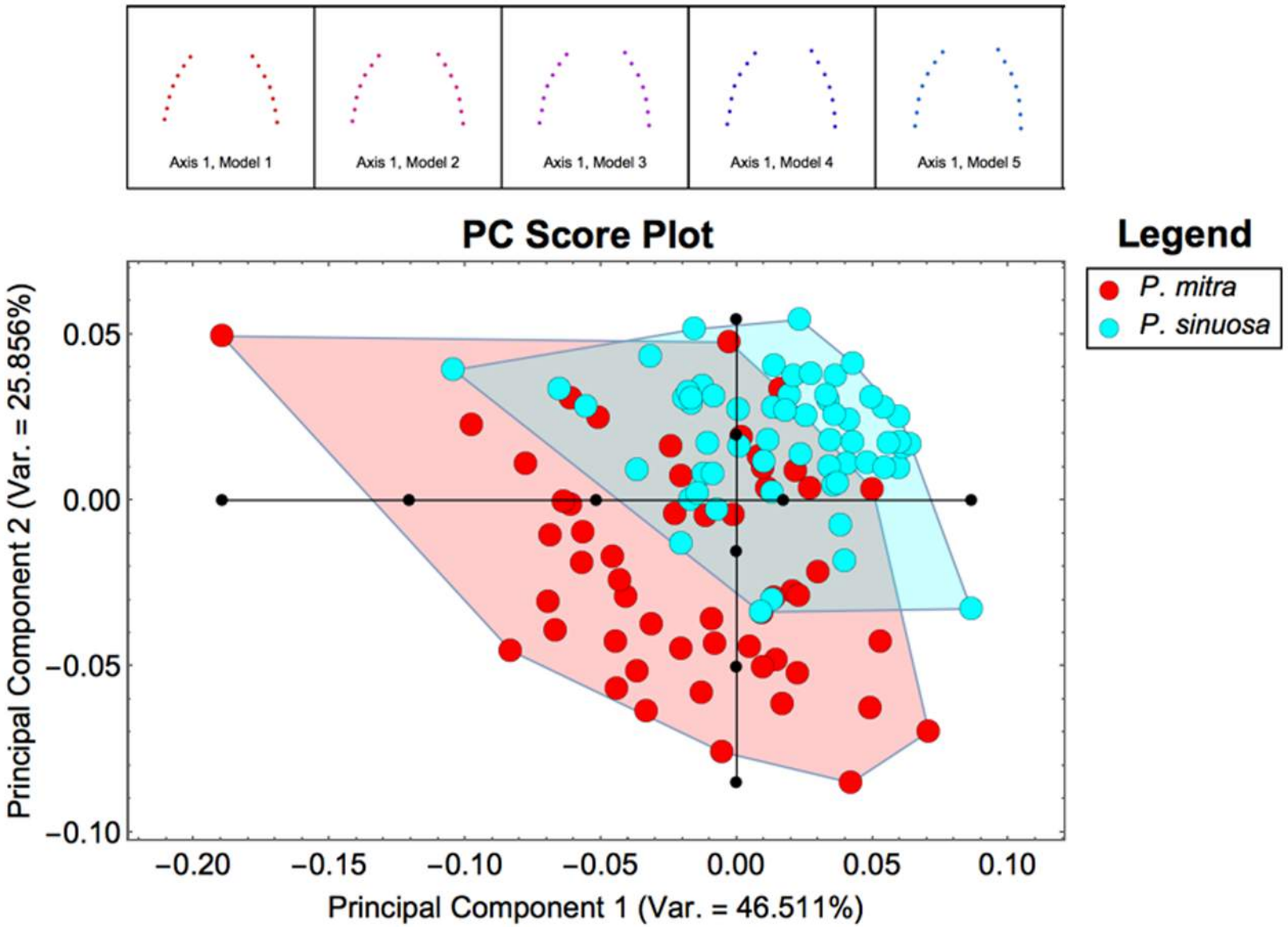
Axis 1, Model 1
Axis 1, Model 2
Axis 1, Model 3
Axis 1, Model 4
Axis 1, Model 5
PC Score Plot
Legend
P. mitra
P. sinuosa
Principal Component 2 (Var. = 25.856%)
0.05
0.00
−0.05
−0.10
−0.20
−0.15
−0.10
−0.05
0.00
0.05
0.10
Principal Component 1 (Var. = 46.511%)

Figure 8

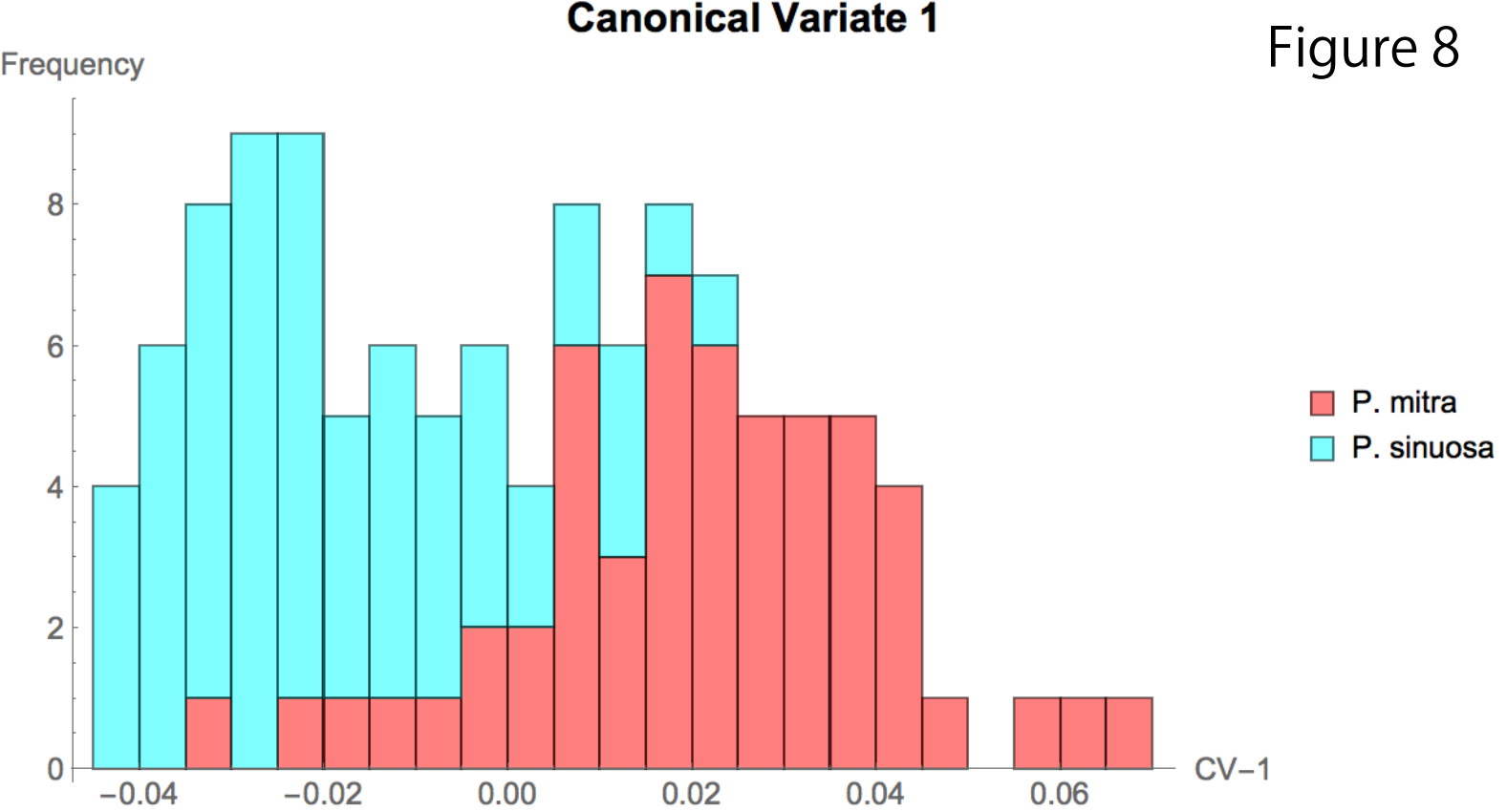
Canonical Variate 1
Frequency
8
6
4
2
0
−0.04
−0.02
0.00
0.02
0.04
0.06
CV−1
P. mitra
P. sinuosa

Figure 9

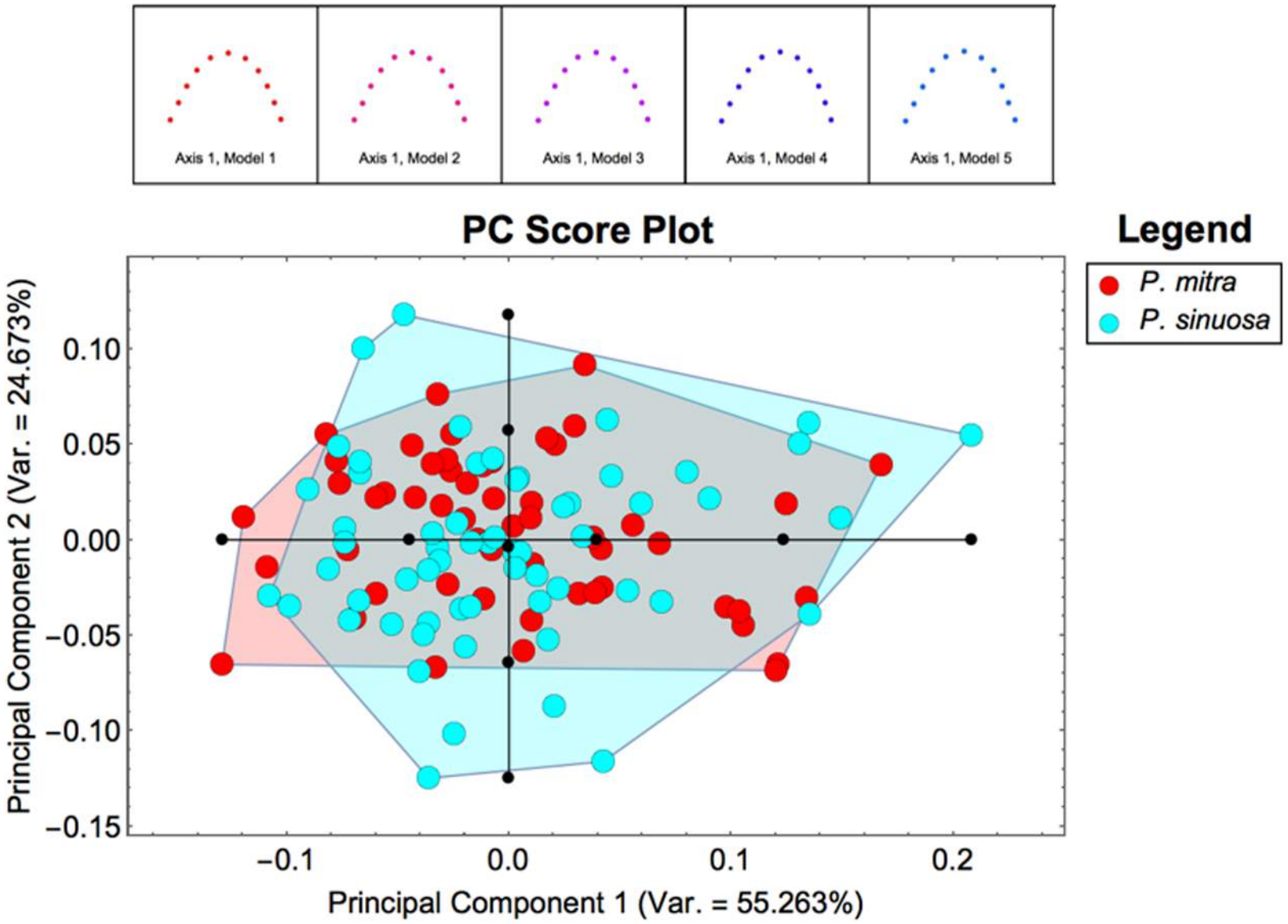
Axis 1, Model 1
Axis 1, Model 2
Axis 1, Model 3
Axis 1, Model 4
Axis 1, Model 5
PC Score Plot
Legend
P. mitra
P. sinuosa
Principal Component 2 (Var. = 24.673%)
0.10
0.05
0.00
−0.05
−0.10
−0.15
−0.1
0.0
0.1
0.2
Principal Component 1 (Var. = 55.263%)

Figure 10

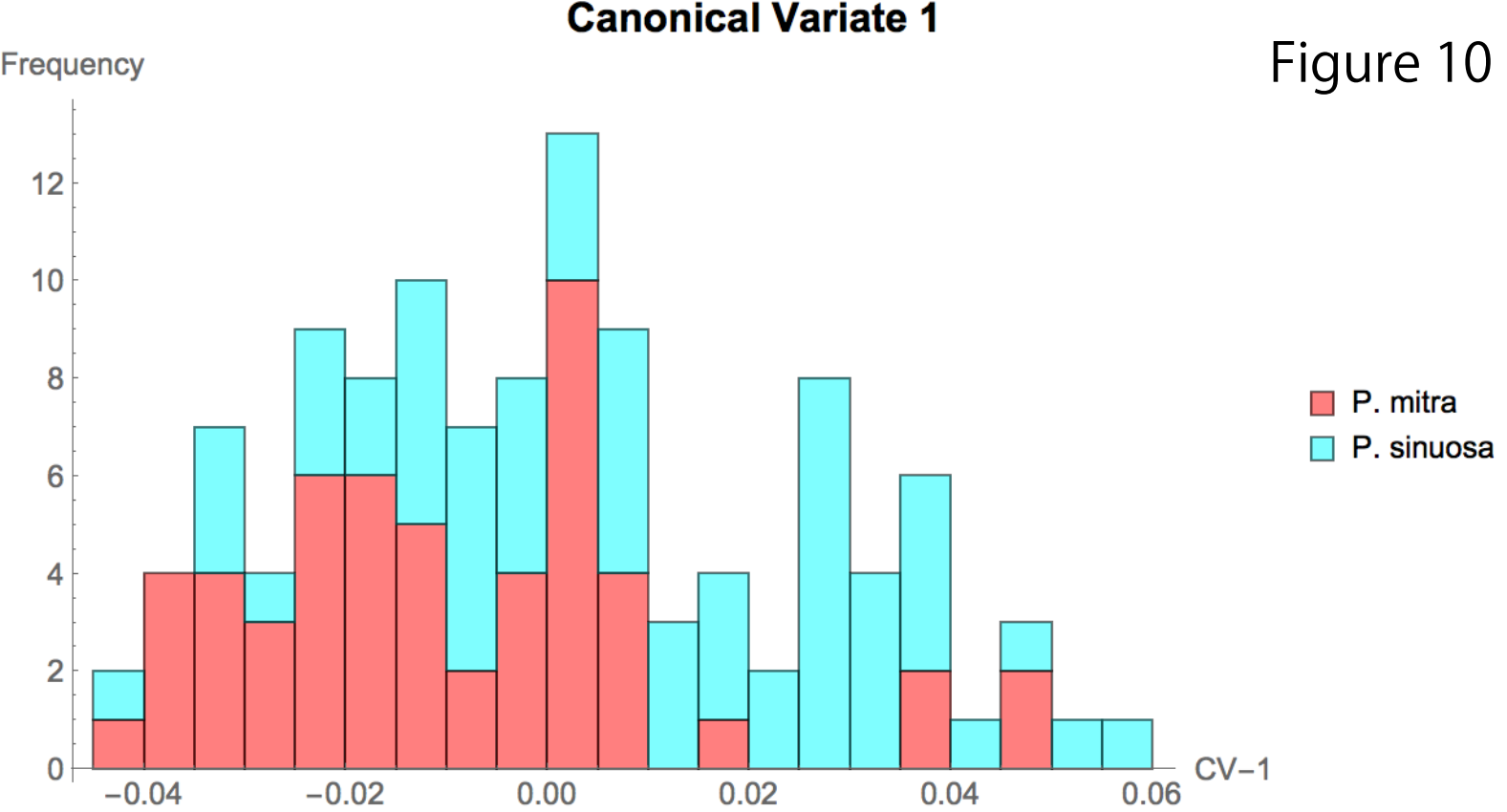
Canonical Variate 1
Frequency
12
10
8
6
4
2
0
−0.04
−0.02
0.00
0.02
0.04
0.06
CV−1
P. mitra
P. sinuosa

Figure 11

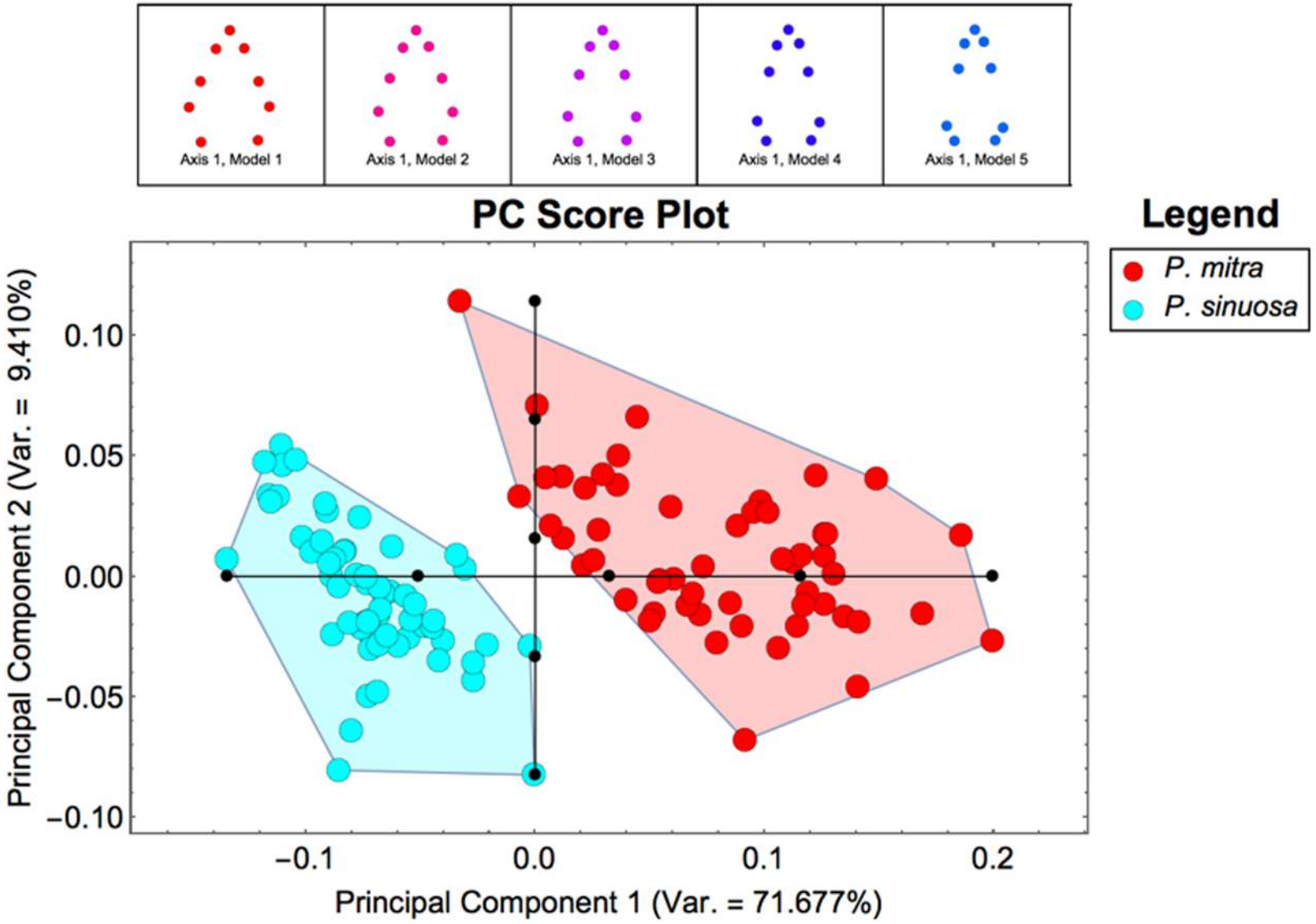
Axis 1, Model 1
Axis 1, Model 2
Axis 1, Model 3
Axis 1, Model 4
Axis 1, Model 5
PC Score Plot
Legend
P. mitra
P. sinuosa
Principal Component 2 (Var. = 9.410%)
0.10
0.05
0.00
−0.05
−0.10
−0.1
0.0
0.1
0.2
Principal Component 1 (Var. = 71.677%)

Figure 12

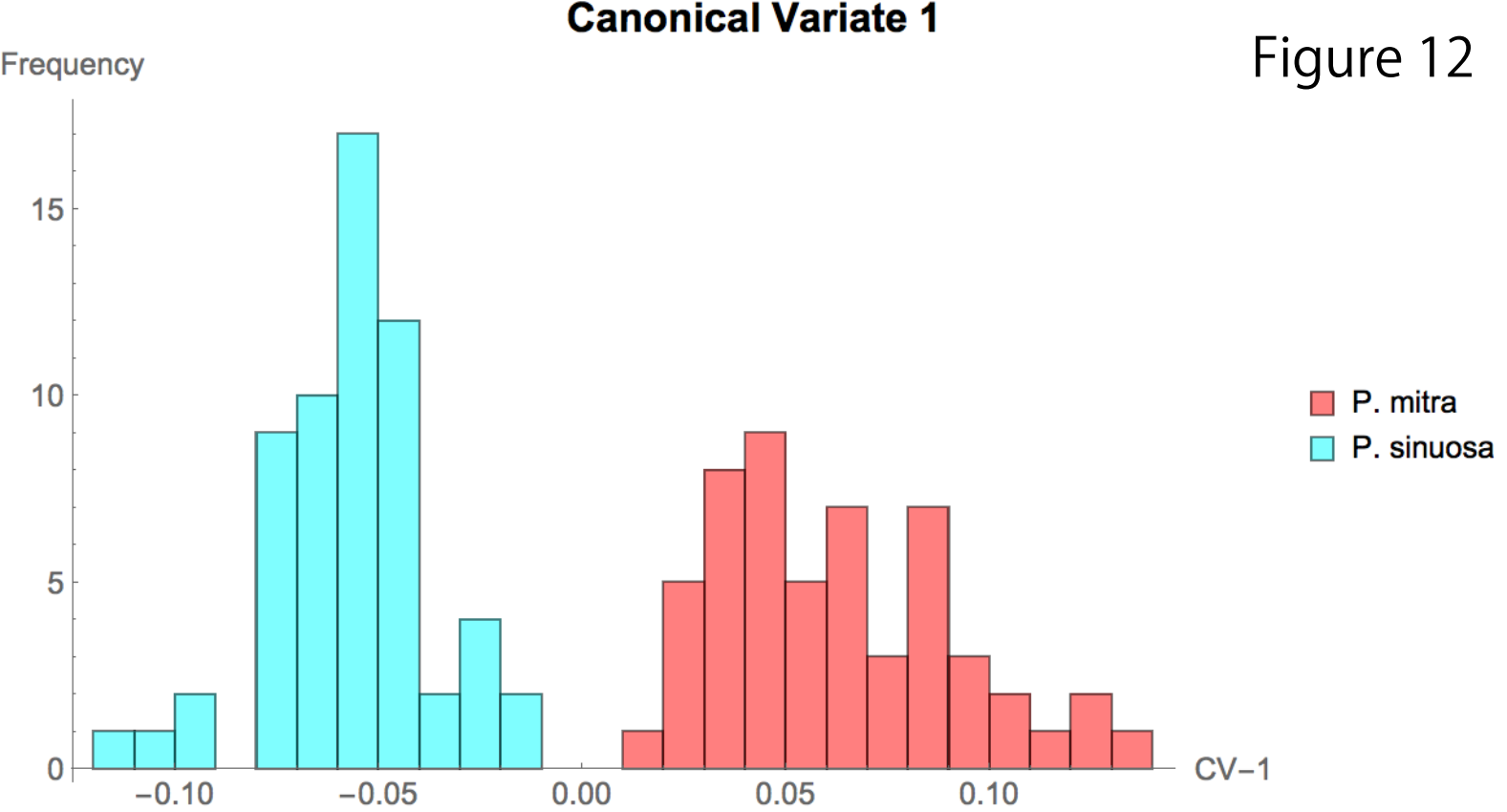
Canonical Variate 1
Frequency
15
10
5
0
−0.10
−0.05
0.00
0.05
0.10
CV−1
P. mitra
P. sinuosa

Table 1 : Stratigraphic horizons, samples and number of specimens

Site	Sample	Biozone	Species	n
709C	35X-01-28cm	upper RP14	P. mitra	33
1259A	21R-cc	upper RP14	P. mitra	11
1259A	24R-cc	RP13/14	P. mitra	10
1259A	24R-cc	RP13/14	P. sinuosa	15
1259A	25R-cc	RP13	P. sinuosa	13
94	21-2-104cm	upper RP12	P. sinuosa	33

All Segments (total outline)

Component	Eigenvalue	Variance (%)	Cum. Variance (%)
1	3.73E-03	62.932	62.932
2	7.09E-04	11.962	74.893
3	3.45E-04	5.816	80.710
4	3.00E-04	5.063	85.773
5	1.84E-04	3.099	88.872
6	1.80E-04	3.035	91.907
7	1.10E-04	1.862	93.769
8	7.78E-05	1.313	95.082
9	6.71E-05	1.131	96.213
10	5.49E-05	0.925	97.139
11	3.58E-05	0.603	97.742
12	2.55E-05	0.431	98.173
13	2.00E-05	0.337	98.510
14	1.48E-05	0.250	98.759
15	1.27E-05	0.215	98.974
16	8.32E-06	0.140	99.114
17	7.78E-06	0.131	99.245
18	6.96E-06	0.117	99.363
19	6.08E-06	0.103	99.465
20	4.56E-06	0.077	99.542
21	3.54E-06	0.060	99.602
22	3.36E-06	0.057	99.659
23	3.09E-06	0.052	99.711
24	2.52E-06	0.043	99.753
25	2.06E-06	0.035	99.788
26	1.71E-06	0.029	99.817
27	1.57E-06	0.027	99.843
28	1.39E-06	0.023	99.867
29	1.18E-06	0.020	99.887
30	9.95E-07	0.017	99.903
31	8.07E-07	0.014	99.917
32	7.75E-07	0.013	99.930
33	6.60E-07	0.011	99.941
34	5.45E-07	0.009	99.950
35	4.74E-07	0.008	99.958
36	3.93E-07	0.007	99.965
37	3.26E-07	0.006	99.971
38	3.21E-07	0.005	99.976
39	2.79E-07	0.005	99.981
40	2.50E-07	0.004	99.985
41	1.56E-07	0.003	99.988
42	1.51E-07	0.003	99.990
43	1.12E-07	0.002	99.992
44	8.94E-08	0.002	99.994
45	6.52E-08	0.001	99.995
46	5.18E-08	0.001	99.995

47	4.17E-08	0.001	99.996
48	3.58E-08	0.001	99.997
49	3.17E-08	0.001	99.997
50	2.54E-08	4.29E-04	99.998
51	1.91E-08	3.22E-04	99.998
52	1.58E-08	2.66E-04	99.998
53	1.33E-08	2.25E-04	99.999
54	1.26E-08	2.12E-04	99.999
55	1.09E-08	1.84E-04	99.999
56	1.02E-08	1.72E-04	99.999
57	8.90E-09	1.50E-04	99.999
58	7.85E-09	1.32E-04	99.999
59	7.13E-09	1.20E-04	100.000
60	6.44E-09	1.09E-04	100.000
61	4.64E-09	7.83E-05	100.000
62	4.13E-09	6.96E-05	100.000
63	3.55E-09	5.99E-05	100.000
64	3.12E-09	5.26E-05	100.000
65	2.31E-09	3.90E-05	100.000
66	1.68E-09	2.84E-05	100.000
67	1.56E-09	2.63E-05	100.000
68	6.79E-20	1.14E-15	100.000
69	-6.71E-20	-1.13E-15	100.000
70	-2.30E-20	-3.88E-16	100.000

Abdomen

Component	Eigenvalue	Variance (%)	Cum. Variance (%)
1	7.17E-03	81.098	81.098
2	7.67E-04	8.674	89.772
3	3.15E-04	3.563	93.335
4	2.26E-04	2.554	95.889
5	1.54E-04	1.739	97.628
6	6.83E-05	0.772	98.400
7	5.41E-05	0.612	99.012
8	2.35E-05	0.266	99.277
9	1.54E-05	0.174	99.451
10	1.44E-05	0.163	99.614
11	9.75E-06	0.110	99.725
12	7.83E-06	0.089	99.813
13	5.76E-06	0.065	99.878
14	4.46E-06	0.050	99.929
15	3.51E-06	0.040	99.969
16	1.48E-06	0.017	99.985
17	4.31E-07	0.005	99.990
18	3.34E-07	0.004	99.994
19	1.69E-07	0.002	99.996
20	1.33E-07	0.002	99.997
21	8.46E-08	0.001	99.998
22	6.33E-08	0.001	99.999
23	3.96E-08	4.48E-04	99.999

24	2.40E-08	2.72E-04	100.000
25	2.15E-08	2.43E-04	100.000
26	-1.91E-19	-2.16E-15	100.000
27	1.55E-19	1.75E-15	100.000
28	2.06E-20	2.33E-16	100.000

Thorax

Component	Eigenvalue	Variance (%)	Cum. Variance (%)
1	1.91E-03	46.511	46.511
2	1.06E-03	25.856	72.367
3	4.85E-04	11.810	84.177
4	3.46E-04	8.421	92.598
5	1.20E-04	2.928	95.526
6	7.23E-05	1.759	97.284
7	3.59E-05	0.874	98.158
8	2.37E-05	0.578	98.736
9	1.52E-05	0.369	99.105
10	8.95E-06	0.218	99.323
11	7.13E-06	0.173	99.497
12	6.31E-06	0.153	99.650
13	5.43E-06	0.132	99.782
14	3.92E-06	0.095	99.878
15	2.60E-06	0.063	99.941
16	1.01E-06	0.025	99.966
17	5.40E-07	0.013	99.979
18	2.24E-07	0.005	99.984
19	1.80E-07	0.004	99.989
20	1.47E-07	0.004	99.992
21	1.21E-07	0.003	99.995
22	7.79E-08	0.002	99.997
23	4.74E-08	0.001	99.998
24	4.64E-08	0.001	99.999
25	3.23E-08	0.001	100.000
26	-6.03E-20	-1.47E-15	100.000
27	-2.04E-20	-4.97E-16	100.000
28	-8.77E-21	-2.13E-16	100.000

Cephalis

Component	Eigenvalue	Variance (%)	Cum. Variance (%)
1	4.30E-03	55.263	55.263
2	1.92E-03	24.673	79.936
3	5.79E-04	7.432	87.368
4	5.54E-04	7.118	94.486
5	1.50E-04	1.929	96.415
6	1.22E-04	1.571	97.986
7	4.73E-05	0.607	98.593
8	4.14E-05	0.531	99.124
9	2.17E-05	0.279	99.403
10	2.00E-05	0.257	99.660
11	1.38E-05	0.178	99.837

12	5.09E-06	0.065	99.903
13	2.91E-06	0.037	99.940
14	1.54E-06	0.020	99.960
15	1.01E-06	0.013	99.973
16	8.80E-07	0.011	99.984
17	5.91E-07	0.008	99.992
18	4.37E-07	0.006	99.997
19	2.00E-07	0.003	100.000
20	1.16E-19	1.49E-15	100.000
21	-3.60E-20	-4.62E-16	100.000
22	1.34E-20	1.72E-16	100.000

Landmarks

Component	Eigenvalue	Variance (%)	Cum. Variance (%)
1	7.41E-03	71.677	71.677
2	9.73E-04	9.410	81.087
3	7.25E-04	7.013	88.100
4	2.87E-04	2.771	90.871
5	1.98E-04	1.913	92.784
6	1.63E-04	1.573	94.357
7	1.32E-04	1.274	95.631
8	1.21E-04	1.170	96.801
9	8.36E-05	0.808	97.609
10	7.72E-05	0.747	98.356
11	6.66E-05	0.644	99.000
12	4.15E-05	0.401	99.401
13	3.16E-05	0.305	99.706
14	2.38E-05	0.231	99.937
15	6.51E-06	0.063	100.000
16	2.06E-19	1.99E-15	100.000
17	7.19E-20	6.95E-16	100.000
18	-1.12E-20	-1.09E-16	100.000

Supplementary Data 2. Results of the Hotelling's T2 test.

	All segments	Abdomen	Thorax	Cephalis	Landmarks
Bootstrap modelling results					
T^2	432.7	268	138.6	17.34	691.3
Observed F-ratio	50.71	65.208	26.738	3.344	93.473
N° of iterations	1000	1000	1000	1000	1000
Probability (%)	0.0	0.0	0.0	0.600	0.0
Parametric Probability results					
T^2	432.7	268	138.6	17.34	691.3
Observed F-ratio	50.71	65.208	26.738	3.344	93.473
Degrees of Freedom 1	8.105	4.109	5.108	5.108	7.106
Probability (%)	1.180×10^{-30}	0.0	0.0	0.757	2.067×10^{-40}